THE JOURNAL OF PHYSICAL CHEMISTRY C
A JOURNAL OF THE AMERICAN CHEMICAL SOCIETY

pubs.acs.org/JPCC

Article

Molecular Dynamics Simulations of Carbon Quantum Dots/Polyamidoamine Dendrimer Nanocomposites

Pawel Wolski,* Tomasz Panczyk, and Agnieszka Brzyska

Cite This: *J. Phys. Chem. C* 2023, 127, 16740−16750

Read Online

ACCESS | Metrics & More | Article Recommendations

ABSTRACT: The covalent modification of carbon quantum dot (CQD) with polyamidoamine (PAMAM) dendrimers was studied using molecular dynamics simulations. Our main objective was to determine how the grafting technique (grafting-from and grafting-to) and the oxidation level of CQD affect the functionalization. We found a series of significant differences in the structure of the CQD-PAMAM nanohybrid depending on the grafting approach and oxidation level of CQD. The "grafting-to" approach reveals a uniform extent of surface coverage by dendrimers, regardless of the oxidation level of CQD. Meanwhile, in the "grafting-from" case, the percentage of surface coverage by dendrimers was strongly determined by the topology of CQD. We also observed that, for a given grafting approach, the increase in the oxidation level of CQD leads to a more compact structure of grafted dendrimers and provides stronger interfacial energy between the two main components of the nanocomposites. Among the interfacial interactions, it was found that the electrostatic force and hydrogen bonding between the charged groups of dendrimers and CQD play a crucial role in controlling the architecture and stability of the formed structures.

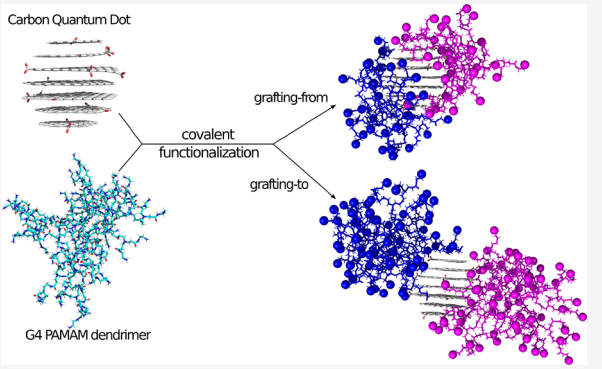

1. INTRODUCTION

Carbon quantum dots (CQDs) are a new type of fluorescent carbon nanostructures with sizes below 10 nm.[1−3] They possess many unique properties, like high solubility, chemical inertness, biocompatibility, low toxicity, excellent photostability, and tunable emission.[4−8] Therefore, in recent years, CQDs have attracted more and more attention in biomedical applications such as biomolecule sensing,[9−15] drug delivery,[16−19] and cell imaging.[20−25] The surface of CQDs contains various functional groups, especially oxygen-related functional groups, such as carboxyl and hydroxyl. Through these reactive groups, diverse kinds of inorganic, organic, polymeric, or biological molecules can be introduced to the CQD surface. In general, surface modification of CQDs with tailored functional ligands can significantly improve their biocompatibility and optical properties, expanding their applications in diagnosis and therapy.[26−33] In the last years, intensive research has been focused on the synthesis of polymer-functionalized CQD-based multifunctional systems.[3,34−38] The functionalization of CQD with different polymers can provide a high surface density of reactive sites for facilitating of attachment of functional molecules and improving solubility in water. In this context, the modification of CQD with branched polymers, i.e., dendrimers, is a promising strategy.[39−42] Dendrimers are hyperbranched macromolecules characterized by a well-ordered, three-dimensional structure and a large number of surface functional groups, which can be easily functionalized, thus modifying their physicochemical or biological properties.[43,44] In particular, polyamidoamine (PAMAM) dendrimers provide a regular structure that linearly increases in diameter and adopts a more globular shape as the dendrimer generation increases.[45] They also contain a large number of available amine sites for conjugation.[46] The several experimental investigations have been performed on nanohybrids of CQDs and PAMAM dendrimers and their applications, most in the biosensors and drug/gene delivery fields.[47−54]

There are two main strategies used for surface modification of CQD: noncovalent and covalent functionalization.[55] Noncovalent modification is based on the physical adsorption of the functional molecules onto the CQD surface through weak interactions, such as electrostatic, van der Waals, and hydrophobic interactions. Noncovalent functionalization provides a simple and mild method for surface modification, preserving the inherent properties of CQDs while improving

Received: July 11, 2023
Revised: July 31, 2023
Published: August 14, 2023

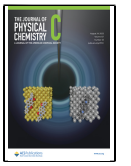

https://doi.org/10.1021/acs.jpcc.3c04661
J. Phys. Chem. C 2023, 127, 16740−16750

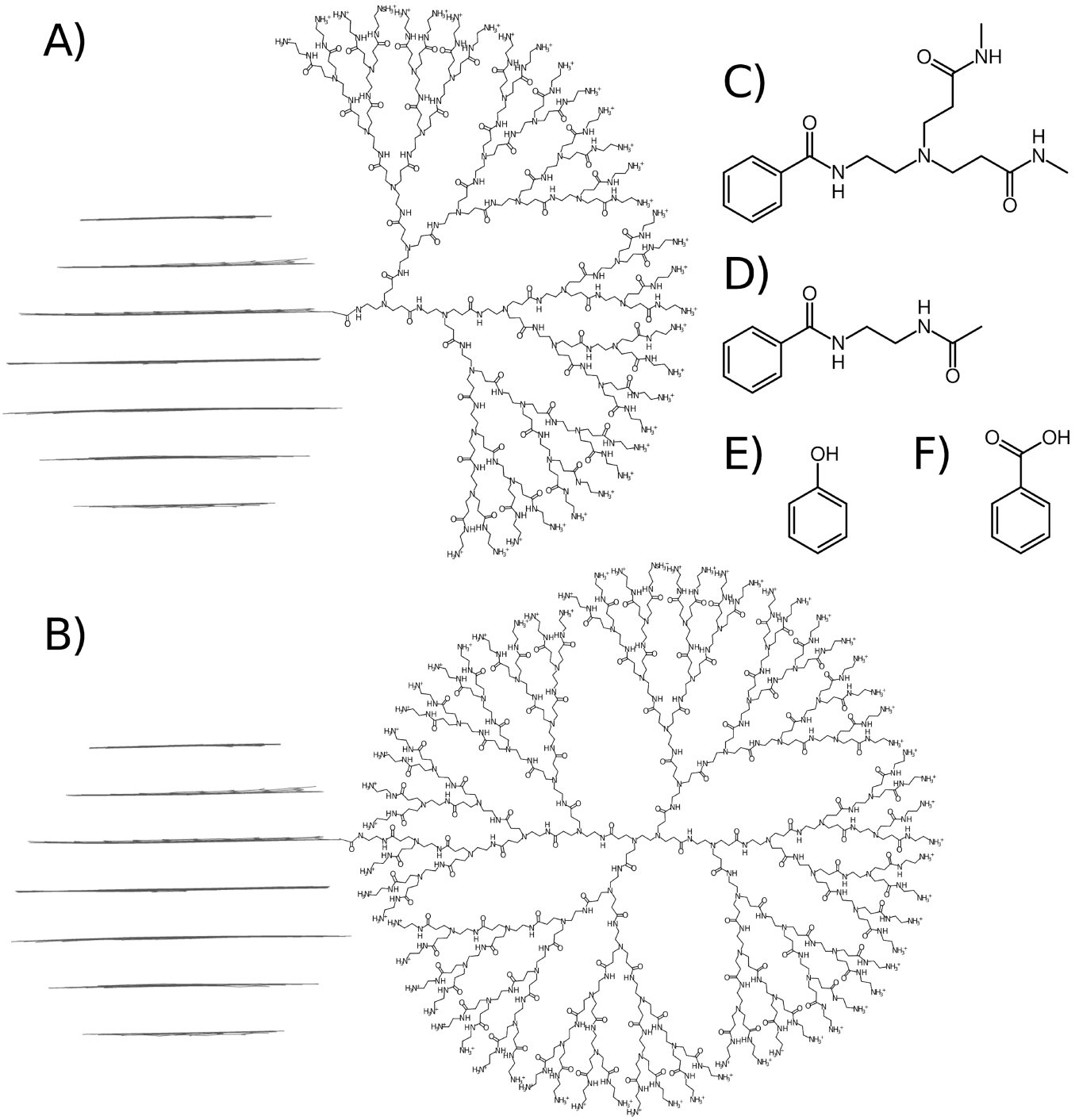

Figure 1. Schematic representation of the covalent functionalization of CQD with PAMAM dendrimer by (A) "grafting-from" and (B) "grafting-to" approaches and parts of the CQD-PAMAM model for which RESP charge derivation was performed (C) grafting-from, (D) grafting-to, (E) hydroxyl functional group of CQD, and (F) carboxyl functional group of CQD.

their biocompatibility and optical properties. Covalent modification involves chemical reactions between the functional molecules and the CQD surface. Compared to the simple physical adsorption, the covalent interactions create a stable nanostructure and allow for better control over the functionalization.[56] The covalent grafting of polymers onto the solid surface can be achieved in practice by "grafting-from" or "grafting-to" approaches[57] (parts A and B of Figure 1). In the "grafting-from" method, polymer chains grow directly from the surface, whereas in "grafting-to", the end-functionalized polymer is attached to the surface.

Despite the promising experimental results, there are still several challenges in preparing decorated CQD surfaces with PAMAM dendrimers. The control over the surface composition and its architecture is essential for the design and development of more efficient CQD−dendrimer nanocomposites with interesting potential in nanotechnology and biomedicine applications. To address these, a thorough atomic-level understanding of the interfacial properties of the

https://doi.org/10.1021/acs.jpcc.3c04661
J. Phys. Chem. C 2023, 127, 16740−16750

dendrimer as well as the dendrimer arrangement near the CQD surface becomes necessary. To the best of our knowledge, there is no molecular dynamics simulation study of PAMAM dendrimers grafted to CQDs. All-atom molecular dynamics simulations are well-suited to gain a microscopic picture of the equilibrium structure and interaction of the PAMAM dendrimers with CQDs.

With this goal in mind, in this study, we used molecular dynamics simulations to investigate the covalent functionalization of CQD with the PAMAM dendrimer of generation 4 at neutral pH. The study focuses on providing in-depth insights into structural features and key aspects of the interfacial interactions between the two main components of the CQD-PAMAM nanohybrid. The effects of the oxidation level of the CQD nanoparticle and two grafting approaches, i.e., "grafting-from" and "grafting-to", on the structure/property relationships of the nanocomposite were examined. The molecular-level information obtained by this study can enable further optimization of the performance of CQD-PAMAM nanohybrids based on a rational design at the microscopic level.

2. METHODS AND MODELS

2.1. Construction of the CQD-G4 PAMAM Model. The initial configurations of CQDs covalently conjugated with poly(amidoamine) (PAMAM) dendrimers via the "grafting-from" and "grafting-to" approaches were constructed according to the following steps. First, the VMD Carbon Dot Builder[58] was used to generate the CQD with ∼19.7 Å diameter of gyration. The created CQD model consists of seven hexagonal graphene-like sheets terminated by hydrogen atoms. Next, the CQD edges were randomly decorated with hydroxyl (−OH) and carboxylic acid (−COOH) functional groups using an in-house script wrapped around the tLeap tool from the AmberTools MD package.[59] The carboxyl-to-hydroxyl group ratio was kept approximately to 2:1. Afterward, another script, which was also based on tLeap software, was used for the covalent link of the dendrimer to the CQD edge. In the case of the "grafting-to" method, the structure of the PAMAM dendrimer of generation 4 (G4) was generated separately and then connected with CQD through one of the polymer end groups (Figure 1B). Thus, within this approach, we get a CQD-full G4 PAMAM complex. Alternatively, in the "grafting-from" approach, the dendrimer structure was sequentially constructed directly from the ethylenediamine core, which was previously anchored to the CQD edge, giving a CQD-half G4 PAMAM complex (Figure 1A). In both cases, the amine group in the core or end moiety of the dendrimer was linked to the CQD edge through the −COOH group (parts C and D of Figure 1). The dendrimer structures were constructed employing the protocol followed in Dendrimer Builder Toolkit (DBT).[60] The GAFF2[61] parameters were used for both the CQDs and dendrimers.

To adjust the charge distribution and force field parameters within the CQD-G4 PAMAM complex, the model was split into several constitutive elements. The dendrimer was divided into three fragments: ethylenediamine core, internal, and surface monomers according to the DBT protocol. To take into account changes in the chemical environment associated with the covalent attachment of the dendrimer to CQD, two additional molecular fragments for core and terminal residue atoms were created. Both these building blocks were capped with a benzene ring to mimic the nearest neighborhood of carbon atoms in the CQD layer to which these groups are linked (parts C and D of Figure 1). In the case of oxygen-containing surface functional groups of CQD, the molecular fragments were actually a phenol molecule, for the −OH functional group (Figure 1E), and a benzoic acid molecule, for the −COOH functional group (Figure 1F). All the fragments were optimized individually using the HF/6-31G* level of theory, and charge distribution was obtained from the restrained electrostatic potential (RESP) method using the R.E.D. server.[62,63] Next, the AMBER GAFF2 force field parameters[61] were derived for all considered molecular fragments using the ACPYPE script.[64] ACPYPE has also been used to port the topology of the final CQD-G4 PAMAM complexes generated in tLeap software to a GROMACS[65] force field format.

The surface of CQDs can be functionalized with a different number of functional groups, which significantly modifies their physicochemical properties. To take this into account in our study, two CQD models were prepared with 10 and 60% edge coverage with oxygen functional groups (carboxyl and hydroxyl). Subsequently, each CQD model was grafted, according to the "grafting-from" and "grafting-to" methods, with two G4-PAMAM dendrimers attached to the opposite side of the nanoparticle. So, in total, we constructed four systems referred to as F-cqd10, F-cqd60, T-cqd10, and T-cqd60, where the first letter of the abbreviation refers to the grafting method and the number at the end to the level of oxidation of CQD. To mimic neutral pH conditions, all the terminal primary amines of dendrimers were considered as protonated.[66] In the case of CQD, all −COOH groups were considered as deprotonated (i.e., $-COO^-$), while the hydroxyl groups were kept protonated.[67]

2.2. Simulations Details. All the simulations were carried out using the GROMACS simulation package.[65] The CQD-G4 PAMAM complex was solvated in an octahedral water box using a TIP3P water model[68] by choosing a 1 nm solvation shell. To neutralize the charges of the CQD-G4 PAMAM complex and to generate the 0.15 M NaCl concentration, an appropriate number of Na^+ and Cl^- ions were added to the system. The solvated complex was then subjected to energy minimization using the steepest descent method. In the next step, the system was gradually heated to 310 K using the V-rescale[69] coupling method in the NVT ensemble, keeping all the heavy atoms on the CQD-G4 PAMAM complex restrained to its starting positions. Subsequently, the equilibration simulation was performed using an NPT ensemble with a Berendsen barostat[70] to maintain pressure isotropically at 1.0 bar. Finally, an unconstrained 200 ns long production run was performed in the NPT ensemble. All simulations were carried out under the periodic boundary conditions. The electrostatic interactions were calculated employing the particle-mesh Ewald[71] method within a cutoff of 12 Å. The same cutoff was used for the van der Waals (vdW) interactions. The LINCS[72] constraints were imposed on all covalent bonds involving hydrogen atoms. Equations of motion were solved using the Verlet leapfrog algorithm,[73] with an integration step of 2 fs.

3. RESULTS AND DISCUSSION

3.1. Structural Characterization of the CQD-G4 PAMAM Nanocomposite. To characterize the effect of the oxidation level of CQD and the grafting approach on the conformation properties of the nanocomposite, we have examined four different CQD-PAMAM models. Overall, the

https://doi.org/10.1021/acs.jpcc.3c04661
J. Phys. Chem. C 2023, 127, 16740−16750

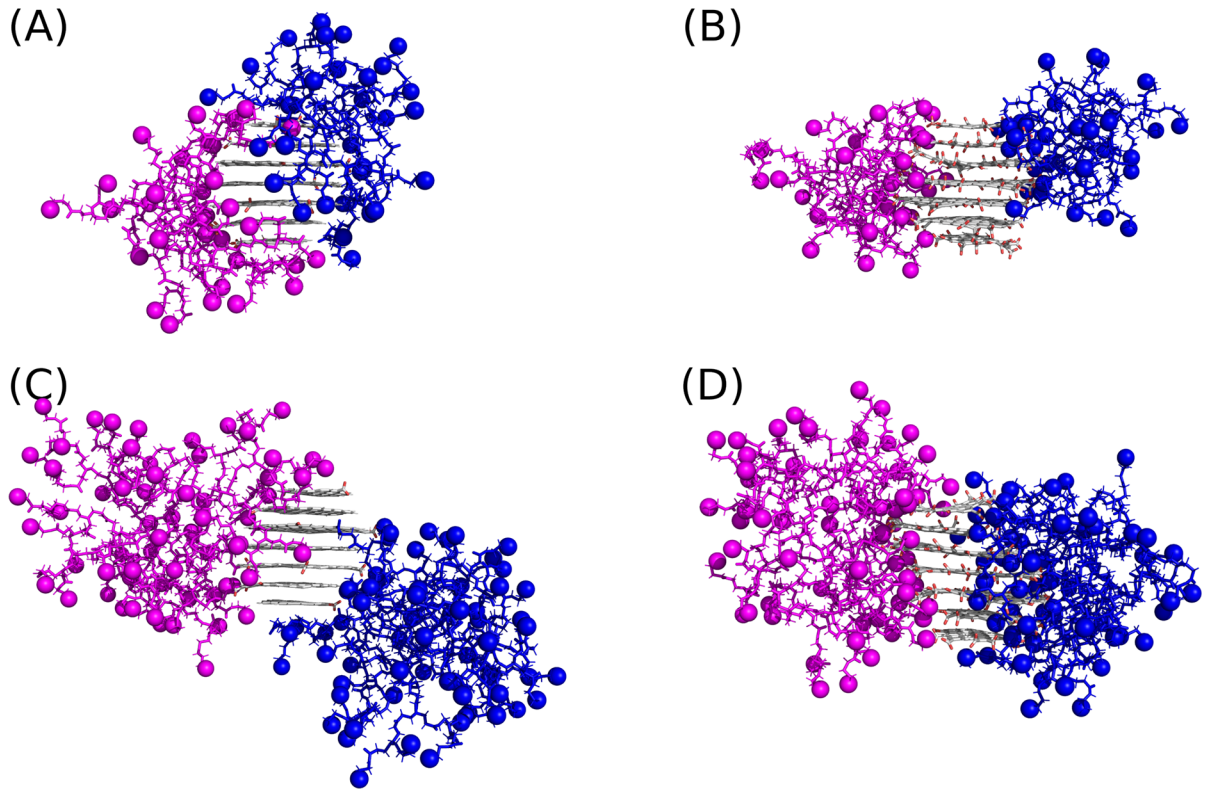

Figure 2. Snapshots of the equilibrated structures of the CQD-G4 PAMAM composites of all the cases studied: (A) F-cqd10, (B) F-cqd60, (C) T-cqd10, and (D) T-cqd60. The CQD nanoparticle is shown in white (with red beads corresponding to oxygen atoms of hydroxyl and carboxyl groups). Dendrimer molecules are shown in magenta and blue. The spheres represent the terminal amines.

conformation of the grafted dendrimers varies between the two grafting methods. Moreover, large differences in the structure of the CQD-G4 PAMAM complexes can also be observed between the two oxidation levels of the CQD for both grafting approaches.

Figure 2 shows the equilibrated structures of the CQD-G4 PAMAM composites. The increase in the number of dendrimer monomers in the "grafting-to" approach makes the height of adsorbed dendrimers greater than in the "grafting-from" case. In comparison to the "grafting-from" approach, the "grafting-to" dendrimers present a more extended conformation. This in turn leads to a larger size of the CQD-G4 PAMAM composite prepared through the "grafting-to" approach. Nevertheless, the differences in the conformations of the grafted dendrimers appear to be greater between the two oxidation levels of CQD than between grafting approaches. In the case of @-cqd10 systems, a large number of dendrimer branches adsorb on the CQD surface, and the remaining monomers rise above it, forming a second layer. In contrast, in @-cqd60 systems, the monomers stay close together and the dendrimers adopt a more compact conformation. Another point to note is that for a given oxidation level of CQD, dendrimers show relatively similar wrapping behavior. For instance, in @-cqd10 systems, the "grafting-from" and "grafting-to" dendrimers coat both the edges and planes of CQDs, while when the oxidation level of the CQD increases, the dendrimers cover mainly the edges of the nanoparticles. Interestingly, for the "grafting-to" approach, although the oxidation level of CQD changes the conformation of grafted dendrimers, this does not seem to affect the surface coverage of nanoparticles by the dendrimers. In both T-cqd@ systems, dendrimers cover a large part of the CQD surface. On the other hand, for the "grafting-from" approach, wrapping efficiency is strongly dependent on the oxidation level of CQD. From parts A and B of Figure 2, one can clearly observe that the dendrimers spread better on the CQD surface in the F-cqd10 case as compared to the F-cqd60 case.

Thus, a visual inspection of Figure 2 suggests that the wrapping nature and conformations of dendrimers adsorbed onto CQD surfaces depend not only on the method used to attach the polymer to the nanoparticle but also on the oxidation level of the substrate. To further determine the spread and conformational change of dendrimers, we calculated the percentage of surface coverage and the radial distribution function.

3.2. Behavior of the CQD in the Nanocomposite. The changes in the CQD geometry, i.e., position of differently composed domains or layer dipole orientation, caused by surface modifications can affect their properties, such as fluorescence. As the CQD has a non-perfect spherical shape (having slightly less height than width), we computed the ratios of the spheroid semiaxes to study the change in the CQD shape. We denote the principal moments of inertia of the gyration tensor of CQD as I_a, I_b, I_c, where $I_a > I_b > I_c$ according to the semiaxes $a < b < c$. This in turn gives

$$c/a = \sqrt{\frac{I_a + I_b - I_c}{I_b + I_c - I_a}} \quad (1)$$

$$b/a = \sqrt{\frac{I_c + I_a - I_b}{I_b + I_c - I_a}} \quad (2)$$

These ratios provide valuable information about the shape of the CQD and its deviation from a perfect sphere. For a perfect

https://doi.org/10.1021/acs.jpcc.3c04661
J. Phys. Chem. C 2023, 127, 16740−16750

sphere, both ratios would be equal to 1. The respective aspect ratios are summarized in Table 1. It may be observed from

Table 1. Comparison of the Ratios of the Spheroid Semiaxes, Size (Radius of Gyration R_g and Actual Radius R), and RMSD of CQD in All Considered Systems

system	c/a	b/c	R_g (R^a) [Å]	RMSD [Å]
F-cqd10	1.17	1.14	9.06 (11.7)	4.43
F-cqd60	1.36	1.29	9.32 (12.04)	2.33
T-cqd10	1.27	1.21	9.11 (11.76)	4.44
T-cqd60	1.92	1.65	9.91 (12.80)	3.22

[a]The actual radius (R) of CQD is related to the radius of gyration of nanoparticle (R_g) through the following relationship $R = \mathrm{sqrt}(5/3) \cdot R_g$.

Table 1 that the CQDs with a higher oxidation level are more asymmetric as compared to those with a lower number of surface groups, irrespective of the grafting approach. As the content of functional groups increases, the CQDs become more elongated. It can be observed from Figure 2 that, in the case of @-cqd60 systems, the horizontal positions of individual sheets fluctuated and shifted from the middle of the sphere. The horizontal shifts of individual layers also increase the radii of gyration (and actual radius) of CQDs. At the same time, for a given oxidation level, it may be observed that the CQDs in the "grafting-from" approach are less aspherical compared to those in the "grafting-to" case, as evident from the values shown in Table 1. This indicates that the "grafting-from" approach is more effective in reducing the horizontal shift of the individual layers in CQD, which may be crucial for particle stability.

The individual layers of CQD can also rotate with respect to each other.[58] The last column of Table 1 shows the average root-mean-square deviation (RMSD) of atomic positions in CQD, which can be used as a measure of its internal motion of the nanoparticle. As can be seen, as the number of oxygen functional groups increases, the RMSD values decrease in both grafting approaches. This alludes that the CQD structure in @-cqd60 systems is less dynamic as compared to @-cqd10 cases. In addition, in the more-oxidized CQD case, the "grafting-from" approach further decreases the internal dynamics of the nanoparticle, whereas in the @-cqd10 cases, the intramolecular kinetics of CQD seems to be not affected by the grafting method.

3.3. Contact Surface Area. Here, the solvent-accessible surface area (SASA) was used to quantify the amount of the CQD surface area covered by the dendrimer for all the studied cases. First, we calculated the SASA of the CQD diminished by the area covered by the grafted dendrimers using the VMD measure sasa command with restrict options. Next, these values were compared with the SASA of the free CQD to obtain a percentage of the CQD area covered by both dendrimers. The average percentage of surface coverage for all systems is plotted in Figure 3.

As seen in Figure 3, the dendrimers in the F-cqd10 system show the highest wrapping tendency of all considered systems. In this case, both dendrimers cover more than 70% of the CQD area. Moreover, values plotted in Figure 3 clearly show that the oxidation level of nanoparticles significantly affects the wrapping efficiency of "grafting-from" dendrimers. As can be seen, in the F-cqd60 system, the increase in the density of oxygen-bearing groups on the CQD surface reduces the area

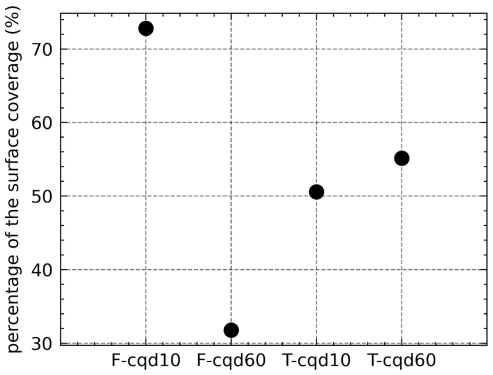

Figure 3. Percentage of the surface coverage of the CQD by dendrimers for the studied cases.

covered by dendrimers to about 32%. From the snapshots in Figure 2, it is clear that protonated primary amine groups tend to interact with oxygenated groups of the CQD. In the F-cqd10 case, the dendrimers spread over the side and graphene sheet regions of the CQD. Such behavior improves the dispersion interactions between the inner branches of dendrimers and the graphene-like regions of the CQD as well as the interactions of primary amine groups with the oxygen-containing groups of the nanoparticles. For the F-cqd60 case, the higher oxidation level of the CQD limits the dispersion interaction between nanoparticles and dendrimers. Moreover, since there are many oxygen functional groups allocated on the CQD sides, dendrimers do not need to spread much over the CQD to interact with them. As a result, we observe a reduction in surface coverage.

In the case of the "grafting-to" approach, the whole dendrimer is attached to the CQD. The increase in the number of dendrimer monomers makes the deformation of the polymer more difficult. As a result, in the "grafting-to" case, the extent of surface coverage by dendrimers is similar between both oxidation levels. In the T-cqd10 and T-cqd60 systems, dendrimers cover 51 and 55% of the CQD surface, respectively. This quantifies the observations from the instantaneous snapshot (Figure 2) that, for the "grafting-to" approach, the surface chemistry of CQDs has a minimal effect on the wrapping efficiency of dendrimers.

Overall, the above results suggest that the "grafting-from" approach is more sensitive to the surface chemistry of CQDs compared to the "grafting-to" approach. Thus, the "grafting-to" method can be more effective for achieving a uniform surface coverage of the CQD, regardless of the number of oxygen functional groups on the surface, than the "grafting-from" technique. On the other hand, it seems that the "grafting-from" technique allows for better control over surface coverage. The maximum or minimum surface can be achieved by tuning the oxidation level of the CQD. Therefore, the "grafting-from" approach may be more suitable for the design of CQD-PAMAM composites with tailored properties.

3.4. Conformations of Grafted Dendrimers. To gain a deeper understanding of the structure and organization of dendrimer layers on the nanoparticle surface, we calculated the radial atomic distribution function (RDF) of dendrimers with respect to the distance to the CQD center of mass. Note that in all RDF plots shown in Figure 4, the origins are set at the center of the mass of the CQD.

From Figure 4, it may be observed that for a given oxidation level of the CQD, the dendrimers show qualitatively similar

https://doi.org/10.1021/acs.jpcc.3c04661
J. Phys. Chem. C 2023, 127, 16740−16750

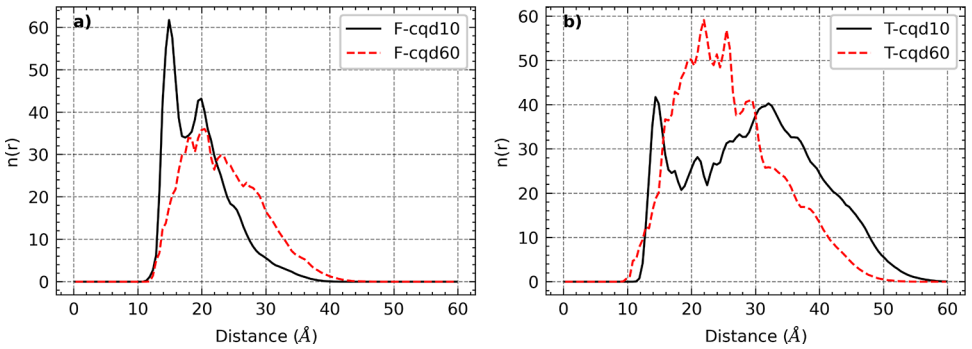

Figure 4. RDF of (a) "grafted-from" and (b) "grafted-to" PAMAM dendrimers with respect to the center of the mass of the CQD.

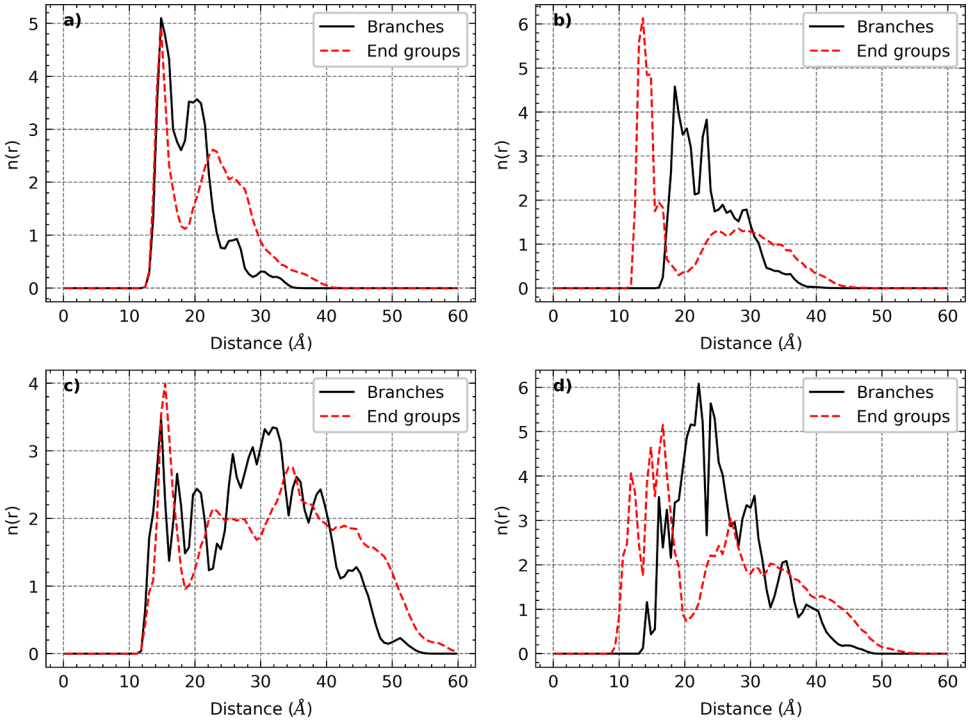

Figure 5. RDF of inner branches and terminal groups of dendrimers with respect to the center of the mass of the CQD in (a) F-cqd10, (b) F-cqd60, (c) T-cqd10, and (d) T-cqd60 systems.

shapes of RDF profiles regardless of the grafting approach. For dendrimers in the @-cqd10 systems (black line in parts a and b of Figure 4), the distributions show a sharp peak located at 14 Å from the center of mass of the nanoparticle, followed by a decrease at an intermediate distance and a subsequent increase in the atom numbers at the periphery. This indicates that there is an adsorbed layer but also a region in which the atoms of the non-adsorbed branches lie. As can be seen from Figure 4, the height of the first peak in the distribution is higher for the F-cqd10 system than for the T-cqd10 case. This implies that more dendrimer branches coat the CQD surface in the former case. This is consistent with the trends from the analysis of the contact surface area that the dendrimers cover a larger surface area of the CQD in the F-cqd10 case than in the T-cqd10 system (see Figure 3). Additionally, for the F-cqd10 case, the narrow spread in the distances of RDF suggests that the dendrimers are tightly packed on the surface, with only a few dendrimer branches rising above the adsorbed layer. This is a clear signature of flat conformation. On the other hand, in the case of the T-cqd10 system, the broader range of the distances in the distribution profile and a well-pronounced second peak at 32 Å indicate that a large number of dendrimer monomers stay away from the surface. As the number of monomers is greater in the "grafting-to" case, the attraction interactions of the CQD may not be strong enough to overcome the steric repulsion between monomers, making the spreading of dendrimers more difficult. Additionally, the primary amines of dendrimers used in this study are protonated, so they may try to minimize the electrostatic repulsion among themselves by lifting some monomers above the adsorbed layer. Hence, in the "grafting-to" approach, the coated dendrimers adopt an expanded brush-like structure. In the "grafting-from" method, a decrease in dendrimer branches leads to a flat configuration in which almost all the monomers of the dendrimers lie on the CQD surface.

In contrast, for the higher oxidation level (red lines in parts a and b of Figure 4), regardless of the grafting approach, the dendrimer distribution profiles show one broadened peak with a "maximum" at about 20 Å, followed by a decrease with increasing distance. A broad maximum, with fluctuations

https://doi.org/10.1021/acs.jpcc.3c04661
J. Phys. Chem. C 2023, 127, 16740−16750

around a constant value, implies that when the oxidation level of the CQD increases, dendrimers adopt a more compact, dense structure. To better understand the molecular origin of these conformational changes, we calculated the distribution of the branching units and terminal groups separately. Figure 5 depicts the radial distribution of the nitrogen atoms of the tertiary amine branches and terminal primary amine groups as a function of the distance from the center of mass of the CQDs. It may be observed that, for both grafting approaches, the location of the maximum distribution of branching units shifts toward larger distances from the CQD with an increase in the oxidation level of the nanoparticle. One can also see that the radial number of terminal groups near the CQD surface in the @-cqd60 systems is higher than in the @-cqd10 cases. As mentioned earlier, the dendrimers have positively charged terminal groups, while the carbonyl groups used to functionalize the surface of the CQD are negatively charged. Thus, an increase in the surface charge of the nanoparticle increases the strength of electrostatic interactions between the protonated amines and CQD. As a result, terminal units move closer to the surface. At the same time, the higher oxidation level limits the interactions with inner branches, which are charge neutral. Therefore, they tend to stay away from the surface, which leads to the dense packing of the coating dendrimers. Such behavior implies that the structure of adsorbed dendrimers can be tuned by modifying the amount of oxygen-bearing groups on the CQD surface.

3.5. Contacts between CQDs and Dendrimers. To further validate the redistribution of the atom positions within the dendrimers, we calculated the fraction of the total number of terminal groups in close contact with the CQD surface. We consider the terminal group to be in contact with the CQD if the distance of separation between the nitrogen atom of the terminal primary amine group and any of the CQD atoms is within 3 Å. This threshold was based on the position of the first peaks in Figure 5 with respect to the actual radius of the CQD (see Table 1). Figure 6 gives the fractional number of

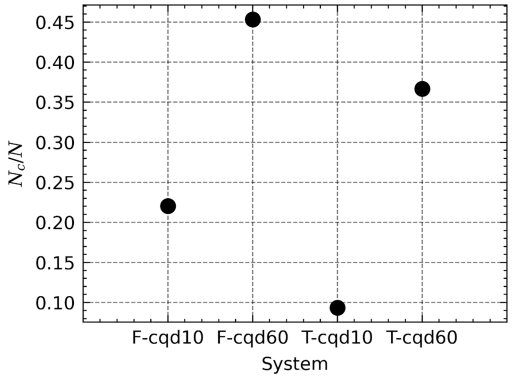

Figure 6. Fractional contacts of the terminal group with the CQD calculated as the ratio of the total number of terminal groups of the dendrimer in contact with the CQD (N_c) to the total number of such groups in the dendrimer.

contacts between the CQD and the terminal groups for all systems under study. It can be noted that for both grafting approaches, the fractional contacts increase as the oxidation level of the CQD increases. This suggests that dendrimers may have greater binding strength when they adsorb on the highly oxidized CQD as compared to the reduced case. Further, for a given oxidation level of the CQD, the "grafting-from" dendrimers make more contacts with the nanoparticle when compared to the "grafting-to" dendrimers. This also suggests that interactions between the CQD and the dendrimer may be greater in the "grafting-from" case as compared to those in the "grafting-to" case.

The conclusions drawn from the fractional contacts are supported by the pair-interaction energies between the CQD and dendrimers. Figure 7 shows the mean pair-interaction

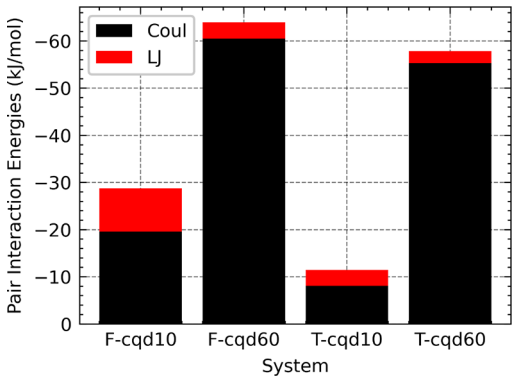

Figure 7. Contribution of electrostatic energy and vdW energy to the total mean pair-interaction energy for all cases.

energies between a single dendrimer monomer and CQD. From this figure, it is clear that the main contribution to the interaction energy comes from the electrostatic component. This demonstrates that the interaction between the dendrimer and the CQD is mainly driven by electrostatic energy. As expected, for a given grafting approach, electrostatic energy and its contribution to the total energy increase as the oxidation level of the CQD increases. Thus, the strongest interaction is observed in the case of @-cqd60 systems. Further, for these systems, a small difference in total energies is observed between the two grafting approaches. On the other hand, in the case of the @-cqd10 systems, the "grafting-from" dendrimers have a higher interaction energy than the "grafting-to" dendrimers. In addition, the F-cqd10 system shows the largest contribution of the vdW interaction to the total energy. This suggests that the F-cqd10 complex is more stable than the T-cqd10 complex. Overall, the T-cqd10 system is the weakest in terms of adsorption strengths when compared to all other cases.

The above results show that electrostatic energy plays a key role in affecting the interfacial interaction energy between the CQD and dendrimers. However, the formation of hydrogen bonds (H-bonds) between the oxygen functional groups located on the CQD surface and dendrimers can also affect the binding strength. Thus, to better understand the interfacial interactions and the effects of the oxidation level of the CQD and the grafting approach on the hydrogen bond interactions, we analyzed the formation of hydrogen bonds between PAMAM dendrimers and CQD. Here, we assume that an H-bond exists when the distance between the acceptor and the donor is smaller than 3 Å and the angle acceptor-donor-H is less than 20 degrees. The calculated detailed information about the hydrogen bonds between the CQD and dendrimers is tabulated in Table 2.

One can expect that the degree of hydrogen bonding will change with the content of functional groups on the CQD surface. Indeed, it can be seen in part A of Table 2 that, for

https://doi.org/10.1021/acs.jpcc.3c04661
J. Phys. Chem. C 2023, 127, 16740−16750

Table 2. Result of the Analysis of the Formation of Hydrogen Bonds between the CQD and PAMAM Dendrimers

panel A: mean number of H-bonds formed between the CQD and dendrimers				
	System			
	F-cqd10	F-cqd60	T-cqd10	T-cqd60
mean number of H-bonds	7.09	20.48	6.50	29.56

panel B: detailed information about the hydrogen bonds[a]			
system	donor	acceptor	frequency of H-bonds (%)
F-cqd10	N4	O	55.22
	N	O	45.83
	N4	O	34.83
	N4	O	32.98
	N	O	31.43
F-cqd60	N4	O	58.67
	N4	O	58.02
	N4	O	57.12
	N4	O	50.17
	N4	O	49.03
T-cqd10	N4	O	38.28
	N	O	36.33
	N	O	25.99
	N	O	21.99
	N4	O	20.59
T-cqd60	N	O	56.72
	N4	O	51.17
	N4	O	49.43
	N4	O	46.78
	N4	O	45.93

[a]N4, nitrogen atom of the terminal primary amine group; N, nitrogen atom of the secondary amine group; O, oxygen atom of the carboxyl group of the CQD.

both grafting approaches, there is an increase in the average number of hydrogen bonds as the oxidation level of the CQD increases. In the @-cqd60 systems, the surface is almost completely covered with oxygen functional groups as compared to the @-cqd10 systems, and hence, the dendrimers can form a larger number of H-bonds. On comparing two grafting techniques, in the @-cqd10 systems, dendrimers form a similar number of H-bonds. On the other hand, in the case of @-cqd60 systems, the "grafting-to" dendrimers form more H-bonds than the "grafting-from" dendrimers. This suggests that for the lower degree of oxidation used in our simulation, the "grafting-from" dendrimers pose enough monomers to achieve a saturated state.

Dendrimers can form different types of hydrogen bonds with the CQD. Panel B of Table 2 shows detailed information about the five most persistent hydrogen bonds formed between the CQD and dendrimers. Analysis of these bonds clearly shows that dendrimers act as hydrogen donors in all cases. For the higher oxidation level of the CQD, the H-bonds are mainly formed with the nitrogen atom of the terminal primary amine group (N4) as the H-bond donor and the oxygen atom of the carboxyl group (O) as the H-bond acceptor. In the case of the @-cqd10 system, we can also observe a second type of H-bond involving the interaction between the secondary amine group (N) and the carboxyl group. Nevertheless, this indicates that H-bonds formed between CQD carboxyl groups and the end groups of dendrimers play a major role in stabilizing the conformation of the adsorbed polymers. In addition, by comparing the interaction frequency of these bonds, it can be concluded that the H-bonds in @cqd60 systems are much stronger than in the case of @-cqd10 systems. Moreover, for a given oxidation level, the H-bonds between the CQD and "grafting-from" dendrimers are stronger than those between "grafting-to" dendrimers. Overall, the above results show that the "grafting-from" approach and high content of carboxyl functional groups improve the interfacial binding energy between the CQD and the dendrimer due to the strong electrostatic and H-bond interactions. Hence, the CQD-modified "grafting-from" approach can provide high structural stability for the CQD-G4 PAMAM composite. The thermodynamics of the binding of dendrimers to CQD will be investigated separately in our future work.

3.6. Dendrimer–Water Interactions. The accessibility of dendrimer functional groups can largely determine the interaction behavior of the entire composite with other molecules. Table 3 shows the average number of H-bonds

Table 3. Average Number of H-Bonds Formed between the Different Kinds of Amine Groups of Dendrimer and Water Molecules for All the Cases

	system			
	F-cqd10	F-cqd60	T-cqd10	T-cqd60
primary amine	0.44	0.32	0.46	0.33
secondary amine	0.06	0.07	0.06	0.06
tertiary amine	0.03	0.07	0.06	0.05
carbonyl	0.33	0.38	0.33	0.34

with water molecules for a single amine (primary, secondary, and tertiary) and carbonyl oxygen. It may be observed that the number of H-bonds formed by primary amines and carbonyl groups is significantly larger than that of secondary and tertiary amines in all cases. Also, for a given grafting approach, the number of H-bonds formed by primary amines decreases with increasing content of oxygen functional groups. As we saw earlier, when the oxidation level of the CQD increases, the protonated primary amine groups move closer to the surface due to favorable interactions with the carboxyl groups. As a result, fewer water molecules can interact with primary amine groups via H-bonding. For the @-cqd10 case, more primary amines stay away from the surface. Thus, it can interact more easily with water molecules. Another point to note is that for a given oxidation level of the CQD, the average number of H-bonds formed between primary amines and water is almost the same for both grafting approaches, showing that the interaction of dendrimers with water molecules is much more affected by the oxidation level of the CQD than by the grafting approach. This suggests that the interaction behavior of the CQD-G4 PAMAM composite with other molecules can be controlled by tuning the polymer–substrate interaction strength.

4. CONCLUSIONS

In this study, the microscopic picture of the CQDs grafted with PAMAM dendrimer generation 4 was investigated using molecular dynamics simulations. We considered two grafting approaches, i.e., "grafting-from" and "grafting-to", as well as two oxidation levels of the CQD. The obtained results revealed that the conformational behavior of the obtained CQD-G4 PAMAM composites depends on the grafting strategy and degree of oxidation of the CQD surface.

https://doi.org/10.1021/acs.jpcc.3c04661
J. Phys. Chem. C 2023, 127, 16740–16750

For the "grafting-from" approach, increasing the oxidation level of the CQD resulted in a reduction in the surface area covered by dendrimers. In contrast, in the "grafting-to" case, the extent of surface coverage by the dendrimer did not depend on the number of oxygen functional groups present on the CQD. In the case of the CQD containing a lower number of functionalized groups, the "grafting-from" dendrimers form a flat, disk-like conformation in which almost all dendrimer branches are adsorbed on the nanoparticle surface. As the number of dendrimer monomers increases in the "grafting-to" approach, dendrimers adopt more expanded conformations, with a large number of monomers rising above the CQD surface. The structure of adsorbed dendrimers becomes more compact when the oxidation level of the CQD increases for both grafting approaches. These characteristic structural features can be attributed to the increasing electrostatic interactions between the protonated primary amine groups of dendrimers and the carboxyl groups of the CQD, which lead to the dense packing of terminal groups close to the CQD surface.

The calculated pair-interaction energies and the number of H-bonds show that the higher oxidation level of the CQD provides stronger interfacial interactions between dendrimers and CQD, regardless of the grafting approach. In addition, the "grafting-from" dendrimers show stronger interactions with CQD as compared to the "grafting-to" cases. From these results, one can conclude that the "grafting-from" coating confers more stability to the final structure of CQD-PAMAM than those obtained by the "grafting-to" approach.

However, most importantly, the redistribution in the position of dendrimer terminal groups, driven by electrostatic and H-bond interactions with the CQD, changes the binding activity of dendrimers with other molecules (water here). This suggests that the surface chemistry of CQDs can be employed as one of the variables to control the interactions between grafted dendrimers and other molecules (e.g., contaminants and drugs) and play a crucial role in an attempt to manage the structure/property relationships of such materials.

We believe that the results of this study on the effects of the grafting approach and oxidation level of the CQD on the surface architecture of dendrimers and their interface with the CQD can have important implications for designing CQD-G4 PAMAM nanocomposites with desired properties for various applications.

AUTHOR INFORMATION

Corresponding Author

Pawel Wolski − *Institute of Catalysis and Surface Chemistry, Polish Academy of Sciences, 30239 Cracow, Poland;* orcid.org/0000-0002-5970-4542; Email: pawel.wolski@ikifp.edu.pl

Authors

Tomasz Panczyk − *Institute of Catalysis and Surface Chemistry, Polish Academy of Sciences, 30239 Cracow, Poland*

Agnieszka Brzyska − *Institute of Catalysis and Surface Chemistry, Polish Academy of Sciences, 30239 Cracow, Poland;* orcid.org/0000-0003-3088-3425

Complete contact information is available at: https://pubs.acs.org/10.1021/acs.jpcc.3c04661

Notes

The authors declare no competing financial interest.

ACKNOWLEDGMENTS

This work was supported by statutory funds of ICSC PAS Poland.

REFERENCES

(1) Wang, F.; Xie, Z.; Zhang, H.; Liu, C.; Zhang, Y. Highly Luminescent Organosilane-Functionalized Carbon Dots. *Adv. Funct. Mater.* **2011**, *21*, 1027−1031.

(2) Baker, S. N.; Baker, G. A. Luminescent Carbon Nanodots: Emergent Nanolights. *Angew. Chem., Int. Ed.* **2010**, *49*, 6726−6744.

(3) Dong, Y.; Wang, R.; Li, H.; Shao, J.; Chi, Y.; Lin, X.; Chen, G. Polyamine-Functionalized Carbon Quantum Dots for Chemical Sensing. *Carbon* **2012**, *50*, 2810−2815.

(4) Yang, S.; Sun, J.; Li, X.; Zhou, W.; Wang, Z.; He, P.; Ding, G.; Xie, X.; Kang, Z.; Jiang, M. Large-Scale Fabrication of Heavy Doped Carbon Quantum Dots with Tunable-Photoluminescence and Sensitive Fluorescence Detection. *J. Mater. Chem. A* **2014**, *2*, 8660−8667.

(5) Guo, H.; Liu, Z.; Shen, X.; Wang, L. One-Pot Synthesis of Orange Emissive Carbon Quantum Dots for All-Type High Color Rendering Index White Light-Emitting Diodes. *ACS Sustainable Chem. Eng.* **2022**, *10*, 8289−8296.

(6) Gu, L.; Zhang, J.; Yang, G.; Tang, Y.; Zhang, X.; Huang, X.; Zhai, W.; Fodjo, E. K.; Kong, C. Green Preparation of Carbon Quantum Dots with Wolfberry as On-off-on Nanosensors for the Detection of Fe3+ and l-Ascorbic Acid. *Food Chem.* **2022**, *376*, No. 131898.

(7) Toma, E. E.; Stoian, G.; Cojocaru, B.; Parvulescu, V. I.; Coman, S. M. ZnO/CQDs Nanocomposites for Visible Light Photodegradation of Organic Pollutants. *Catalysts* **2022**, *12*, 952.

(8) Ray, S. C.; Saha, A.; Jana, N. R.; Sarkar, R. Fluorescent Carbon Nanoparticles: Synthesis, Characterization, and Bioimaging Application. *J. Phys. Chem. C* **2009**, *113*, 18546−18551.

(9) Anjana, R. R.; Anjali Devi, J. S.; Jayasree, M.; Aparna, R. S.; Aswathy, B.; Praveen, G. L.; Lekha, G. M.; Sony, G. S,N-Doped Carbon Dots as a Fluorescent Probe for Bilirubin. *Microchim. Acta* **2018**, *185*, 11.

(10) Zhou, L.; Lin, Y.; Huang, Z.; Ren, J.; Qu, X. Carbon Nanodots as Fluorescence Probes for Rapid, Sensitive, and Label-Free Detection of Hg 2+ and Biothiols in Complex Matrices. *Chem. Commun.* **2012**, *48*, 1147−1149.

(11) Lin, Z.; Xue, W.; Chen, H.; Lin, J.-M. Peroxynitrous-Acid-Induced Chemiluminescence of Fluorescent Carbon Dots for Nitrite Sensing. *Anal. Chem.* **2011**, *83*, 8245−8251.

(12) Bai, W.; Zheng, H.; Long, Y.; Mao, X.; Gao, M.; Zhang, L. A Carbon Dots-Based Fluorescence Turn-on Method for DNA Determination. *Anal. Sci.* **2011**, *27*, 243−246.

(13) Zhao, J.; Chen, G.; Zhu, L.; Li, G. Graphene Quantum Dots-Based Platform for the Fabrication of Electrochemical Biosensors. *Electrochem. Commun.* **2011**, *13*, 31−33.

(14) López, C.; Zougagh, M.; Algarra, M.; Rodríguez-Castellón, E.; Campos, B. B.; Esteves da Silva, J. C. G.; Jiménez-Jiménez, J.; Ríos, A. Microwave-Assisted Synthesis of Carbon Dots and Its Potential as Analysis of Four Heterocyclic Aromatic Amines. *Talanta* **2015**, *132*, 845−850.

(15) Algarra, M.; Campos, B. B.; Radotić, K.; Mutavdžić, D.; Bandosz, T.; Jiménez-Jiménez, J.; Rodriguez-Castellón, E.; Da Silva, J. C. G. E. Luminescent Carbon Nanoparticles: Effects of Chemical Functionalization, and Evaluation of Ag+ Sensing Properties. *J. Mater. Chem. A* **2014**, *2*, 8342−8351.

(16) Karthik, S.; Saha, B.; Ghosh, S. K.; Singh, N. D. P. Photoresponsive Quinoline Tethered Fluorescent Carbon Dots for Regulated Anticancer Drug Delivery. *Chem. Commun.* **2013**, *49*, 10471−10473.

(17) Wang, Q.; Huang, X.; Long, Y.; Wang, X.; Zhang, H.; Zhu, R.; Liang, L.; Teng, P.; Zheng, H. Hollow Luminescent Carbon Dots for Drug Delivery. *Carbon* **2013**, *59*, 192−199.
(18) Wang, H.; Shen, J.; Li, Y.; Wei, Z.; Cao, G.; Gai, Z.; Hong, K.; Banerjee, P.; Zhou, S. Magnetic Iron Oxide−Fluorescent Carbon Dots Integrated Nanoparticles for Dual-Modal Imaging, near-Infrared Light-Responsive Drug Carrier and Photothermal Therapy. *Biomater. Sci.* **2014**, *2*, 915−923.
(19) Pardo, J.; Peng, Z.; Leblanc, R. M. Cancer Targeting and Drug Delivery Using Carbon-Based Quantum Dots and Nanotubes. *Molecules* **2018**, *23*, 378.
(20) Zhou, J.; Zhou, H.; Tang, J.; Deng, S.; Yan, F.; Li, W.; Qu, M. Carbon Dots Doped with Heteroatoms for Fluorescent Bioimaging: A Review. *Microchim. Acta* **2017**, *184*, 343−368.
(21) Dong, J.; Wang, K.; Sun, L.; Sun, B.; Yang, M.; Chen, H.; Wang, Y.; Sun, J.; Dong, L. Application of Graphene Quantum Dots for Simultaneous Fluorescence Imaging and Tumor-Targeted Drug Delivery. *Sens. Actuators, B* **2018**, *256*, 616−623.
(22) Ding, C.; Zhu, A.; Tian, Y. Functional Surface Engineering of C-Dots for Fluorescent Biosensing and in Vivo Bioimaging. *Acc. Chem. Res.* **2014**, *47*, 20−30.
(23) Bhunia, S. K.; Saha, A.; Maity, A. R.; Ray, S. C.; Jana, N. R. Carbon Nanoparticle-Based Fluorescent Bioimaging Probes. *Sci. Rep.* **2013**, *3*, 1473.
(24) Li, Q.; Ohulchanskyy, T. Y.; Liu, R.; Koynov, K.; Wu, D.; Best, A.; Kumar, R.; Bonoiu, A.; Prasad, P. N. Photoluminescent Carbon Dots as Biocompatible Nanoprobes for Targeting Cancer Cells in Vitro. *J. Phys. Chem. C* **2010**, *114*, 12062−12068.
(25) Hola, K.; Zhang, Y.; Wang, Y.; Giannelis, E. P.; Zboril, R.; Rogach, A. L. Carbon Dots—Emerging Light Emitters for Bioimaging Cancer Therapy and Optoelectronics. *Nano Today* **2014**, *9*, 590−603.
(26) Yang, S.-T.; Wang, X.; Wang, H.; Lu, F.; Luo, P. G.; Cao, L.; Meziani, M. J.; Liu, J.-H.; Liu, Y.; Chen, M.; Huang, Y.; Sun, Y.-P. Carbon Dots as Nontoxic and High-Performance Fluorescence Imaging Agents. *J. Phys. Chem. C* **2009**, *113*, 18110−18114.
(27) Wang, X.; Cao, L.; Yang, S.-T.; Lu, F.; Meziani, M. J.; Tian, L.; Sun, K. W.; Bloodgood, M. A.; Sun, Y.-P. Bandgap-Like Strong Fluorescence in Functionalized Carbon Nanoparticles. *Angew. Chem., Int. Ed.* **2010**, *49*, 5310−5314.
(28) Van Tam, T.; Ho Hong, S.; Mook Choi, W. Facile Synthesis of Cysteine−Functionalized Graphene Quantum Dots for a Fluorescence Probe for Mercury Ions. *RSC Adv.* **2015**, *5*, 97598−97603.
(29) Wang, Z.; Wang, F.; Zhu, Y.; Gong, B. Method of Desulfurization Process Selection Based on Improved Fuzzy Comprehensive Evaluation: A Case Study of Papermaking Desulfurization in China. *Processes* **2019**, *7*, 446.
(30) Liu, R.; Zhang, L.; Zhao, J.; Luo, Z.; Huang, Y.; Zhao, S. Aptamer and IR820 Dual-Functionalized Carbon Dots for Targeted Cancer Therapy against Hypoxic Tumors Based on an 808 Nm Laser-Triggered Three-Pathway Strategy. *Adv. Ther.* **2018**, *1*, 1800041.
(31) Mewada, A.; Pandey, S.; Thakur, M.; Jadhav, D.; Sharon, M. Swarming Carbon Dots for Folic Acid Mediated Delivery of Doxorubicin and Biological Imaging. *J. Mater. Chem. B* **2014**, *2*, 698−705.
(32) Zhao, X.; Zhang, J.; Shi, L.; Xian, M.; Dong, C.; Shuang, S. Folic Acid-Conjugated Carbon Dots as Green Fluorescent Probes Based on Cellular Targeting Imaging for Recognizing Cancer Cells. *RSC Adv.* **2017**, *7*, 42159−42167.
(33) Hai, X.; Wang, Y.; Hao, X.; Chen, X.; Wang, J. Folic Acid Encapsulated Graphene Quantum Dots for Ratiometric PH Sensing and Specific Multicolor Imaging in Living Cells. *Sens. Actuators, B* **2018**, *268*, 61−69.
(34) Yang, S.-T.; Cao, L.; Luo, P. G.; Lu, F.; Wang, X.; Wang, H.; Meziani, M. J.; Liu, Y.; Qi, G.; Sun, Y.-P. Carbon Dots for Optical Imaging in Vivo. *J. Am. Chem. Soc.* **2009**, *131*, 11308−11309.
(35) Wang, Y.; Anilkumar, P.; Cao, L.; Liu, J.-H.; Luo, P. G.; Tackett, K. N.; Sahu, S.; Wang, P.; Wang, X.; Sun, Y.-P. Carbon Dots of Different Composition and Surface Functionalization: Cytotoxicity Issues Relevant to Fluorescence Cell Imaging. *Exp. Biol. Med.* **2011**, *236*, 1231−1238.
(36) Wang, W.; Li, Y.; Cheng, L.; Cao, Z.; Liu, W. Water-Soluble and Phosphorus-Containing Carbon Dots with Strong Green Fluorescence for Cell Labeling. *J. Mater. Chem. B* **2014**, *2*, 46−48.
(37) Liu, C.; Zhang, P.; Zhai, X.; Tian, F.; Li, W.; Yang, J.; Liu, Y.; Wang, H.; Wang, W.; Liu, W. Nano-Carrier for Gene Delivery and Bioimaging Based on Carbon Dots with PEI-Passivation Enhanced Fluorescence. *Biomaterials* **2012**, *33*, 3604−3613.
(38) Cao, L.; Wang, X.; Meziani, M. J.; Lu, F.; Wang, H.; Luo, P. G.; Lin, Y.; Harruff, B. A.; Veca, L. M.; Murray, D.; Xie, S.-Y.; Sun, Y.-P. Carbon Dots for Multiphoton Bioimaging. *J. Am. Chem. Soc.* **2007**, *129*, 11318−11319.
(39) Sato, K.; Anzai, J. Dendrimers in Layer-by-Layer Assemblies: Synthesis and Applications. *Molecules* **2013**, *18*, 8440−8460.
(40) Wang, Q.; Liu, X.; Zhang, L.; Lv, Y. Microwave-Assisted Synthesis of Carbon Nanodots through an Eggshell Membrane and Their Fluorescent Application. *Analyst* **2012**, *137*, 5392−5397.
(41) Dong, Y.; Wang, R.; Li, G.; Chen, C.; Chi, Y.; Chen, G. Polyamine-Functionalized Carbon Quantum Dots as Fluorescent Probes for Selective and Sensitive Detection of Copper Ions. *Anal. Chem.* **2012**, *84*, 6220−6224.
(42) Liu, Y.; Hu, J.; Li, Y.; Wei, H.-P.; Li, X.-S.; Zhang, X.-H.; Chen, S.-M.; Chen, X.-Q. Synthesis of Polyethyleneimine Capped Carbon Dots for Preconcentration and Slurry Sampling Analysis of Trace Chromium in Environmental Water Samples. *Talanta* **2015**, *134*, 16−23.
(43) Bosman, A. W.; Janssen, H. M.; Meijer, E. W. About Dendrimers: Structure, Physical Properties, and Applications. *Chem. Rev.* **1999**, *99*, 1665−1688.
(44) Kim, Y.; Zimmerman, S. C. Applications of Dendrimers in Bio-Organic Chemistry. *Curr. Opin. Chem. Biol.* **1998**, *2*, 733−742.
(45) Esfand, R.; Tomalia, D. A. Poly(Amidoamine) (PAMAM) Dendrimers: From Biomimicry to Drug Delivery and Biomedical Applications. *Drug Discovery Today* **2001**, *6*, 427−436.
(46) Astruc, D.; Boisselier, E.; Ornelas, C. Dendrimers Designed for Functions: From Physical, Photophysical, and Supramolecular Properties to Applications in Sensing, Catalysis, Molecular Electronics, Photonics, and Nanomedicine. *Chem. Rev.* **2010**, *110*, 1857−1959.
(47) Ngu-Schwemlein, M.; Chin, S. F.; Hileman, R.; Drozdowski, C.; Upchurch, C.; Hargrove, A. Carbon Nanodots as Molecular Scaffolds for Development of Antimicrobial Agents. *Bioorg. Med. Chem. Lett.* **2016**, *26*, 1745−1749.
(48) Zong, J.; Yang, X.; Trinchi, A.; Hardin, S.; Cole, I.; Zhu, Y.; Li, C.; Muster, T.; Wei, G. Photoluminescence Enhancement of Carbon Dots by Gold Nanoparticles Conjugated via PAMAM Dendrimers. *Nanoscale* **2013**, *5*, 11200−11206.
(49) Campos, B. B.; Oliva, M. M.; Contreras-Cáceres, R.; Rodriguez-Castellón, E.; Jiménez-Jiménez, J.; da Silva, J. C. G. E.; Algarra, M. Carbon Dots on Based Folic Acid Coated with PAMAM Dendrimer as Platform for Pt(IV) Detection. *J. Colloid Interface Sci.* **2016**, *465*, 165−173.
(50) Lin, T. N.; Inciong, M. R.; Santiago, S. R.; Kao, C. W.; Shu, G. W.; Yuan, C. T.; Shen, J. L.; Yeh, J. M.; Chen-Yang, Y. W. Electron Injection from Graphene Quantum Dots to Poly(Amido Amine) Dendrimers. *Appl. Phys. Lett.* **2016**, *108*, No. 161904.
(51) Li, D.; Fan, Y.; Shen, M.; Bányai, I.; Shi, X. Design of Dual Drug-Loaded Dendrimer/Carbon Dot Nanohybrids for Fluorescence Imaging and Enhanced Chemotherapy of Cancer Cells. *J. Mater. Chem. B* **2019**, *7*, 277−285.
(52) Bhatnagar, D.; Kaur, I.; Kumar, A. Ultrasensitive Cardiac Troponin I Antibody Based Nanohybrid Sensor for Rapid Detection of Human Heart Attack. *Int. J. Biol. Macromol.* **2017**, *95*, 505−510.
(53) Ghosh, S.; Ghosal, K.; Mohammad, S. A.; Sarkar, K. Dendrimer Functionalized Carbon Quantum Dot for Selective Detection of Breast Cancer and Gene Therapy. *Chem. Eng. J.* **2019**, *373*, 468−484.
(54) Martins, I.; Tomás, H.; Lahoz, F.; Rodrigues, J. Engineered Fluorescent Carbon Dots and G4-G6 PAMAM Dendrimer Nano-

https://doi.org/10.1021/acs.jpcc.3c04661
J. Phys. Chem. C 2023, 127, 16740−16750

hybrids for Bioimaging and Gene Delivery. *Biomacromolecules* **2021**, *22*, 2436−2450.
(55) Pirsaheb, M.; Mohammadi, S.; Salimi, A.; Payandeh, M. Functionalized Fluorescent Carbon Nanostructures for Targeted Imaging of Cancer Cells: A Review. *Microchim. Acta* **2019**, *186*, 231.
(56) Conzatti, G.; Cavalie, S.; Combes, C.; Torrisani, J.; Carrere, N.; Tourrette, A. PNIPAM Grafted Surfaces through ATRP and RAFT Polymerization: Chemistry and Bioadhesion. *Colloids Surf., B* **2017**, *151*, 143−155.
(57) Minko, S. Grafting on Solid Surfaces: "Grafting to" and "Grafting from" Methods. In *Polymer Surfaces and Interfaces: Characterization, Modification and Applications*; Stamm, M., Ed.; Springer: Berlin, Heidelberg, 2008; pp. 215−234, DOI: 10.1007/978-3-540-73865-7_11.
(58) Paloncýová, M.; Langer, M.; Otyepka, M. Structural Dynamics of Carbon Dots in Water and N,N-Dimethylformamide Probed by All-Atom Molecular Dynamics Simulations. *J. Chem. Theory Comput.* **2018**, *14*, 2076−2083.
(59) Case, D. A.; Cheatham, T. E., III; Darden, T.; Gohlke, H.; Luo, R.; Merz, K. M., Jr.; Onufriev, A.; Simmerling, C.; Wang, B.; Woods, R. J. The Amber Biomolecular Simulation Programs. *J. Comput. Chem.* **2005**, *26*, 1668−1688.
(60) Maingi, V.; Jain, V.; Bharatam, P. V.; Maiti, P. K. Dendrimer Building Toolkit: Model Building and Characterization of Various Dendrimer Architectures. *J. Comput. Chem.* **2012**, *33*, 1997−2011.
(61) Wang, J.; Wolf, R. M.; Caldwell, J. W.; Kollman, P. A.; Case, D. A. Development and Testing of a General Amber Force Field. *J. Comput. Chem.* **2004**, *25*, 1157−1174.
(62) Vanquelef, E.; Simon, S.; Marquant, G.; Garcia, E.; Klimerak, G.; Delepine, J. C.; Cieplak, P.; Dupradeau, F.-Y. R. E. D. Server: A Web Service for Deriving RESP and ESP Charges and Building Force Field Libraries for New Molecules and Molecular Fragments. *Nucleic Acids Res.* **2011**, *39*, W511−W517.
(63) Dupradeau, F.-Y.; Pigache, A.; Zaffran, T.; Savineau, C.; Lelong, R.; Grivel, N.; Lelong, D.; Rosanski, W.; Cieplak, P. The R.E.D. Tools: Advances in RESP and ESP Charge Derivation and Force Field Library Building. *Phys. Chem. Chem. Phys.* **2010**, *12*, 7821−7839.
(64) Sousa da Silva, A. W.; Vranken, W. F. A. C. P. Y. P. E. AnteChamber PYthon Parser InterfacE. *BMC Res Notes* **2012**, *5*, 367.
(65) Abraham, M. J.; Murtola, T.; Schulz, R.; Páll, S.; Smith, J. C.; Hess, B.; Lindahl, E. GROMACS: High Performance Molecular Simulations through Multi-Level Parallelism from Laptops to Supercomputers. *SoftwareX* **2015**, *1-2*, 19−25.
(66) Cakara, D.; Kleimann, J.; Borkovec, M. Microscopic Protonation Equilibria of Poly(Amidoamine) Dendrimers from Macroscopic Titrations. *Macromolecules* **2003**, *36*, 4201−4207.
(67) Konkena, B.; Vasudevan, S. Understanding Aqueous Dispersibility of Graphene Oxide and Reduced Graphene Oxide through PKa Measurements. *The Journal of Physical Chemistry Letters* **2012**, *3*, 867−872.
(68) Jorgensen, W. L.; Chandrasekhar, J.; Madura, J. D.; Impey, R. W.; Klein, M. L. Comparison of Simple Potential Functions for Simulating Liquid Water. *J. Chem. Phys.* **1983**, *79*, 926−935.
(69) Bussi, G.; Donadio, D.; Parrinello, M. Canonical Sampling through Velocity Rescaling. *J. Chem. Phys.* **2007**, *126*, No. 014101.
(70) Berendsen, H. J. C.; Postma, J. P. M.; van Gunsteren, W. F.; DiNola, A.; Haak, J. R. Molecular Dynamics with Coupling to an External Bath. *J. Chem. Phys.* **1984**, *81*, 3684−3690.
(71) Darden, T.; York, D.; Pedersen, L. Particle Mesh Ewald: An N·log(N) Method for Ewald Sums in Large Systems. *J. Chem. Phys.* **1993**, *98*, 10089−10092.
(72) Hess, B.; Bekker, H.; Berendsen, H. J. C.; Fraaije, J. G. E. M. LINCS: A Linear Constraint Solver for Molecular Simulations. *J. Comput. Chem.* **1997**, *18*, 1463−1472.
(73) Hockney, R. W.; Goel, S. P.; Eastwood, J. W. Quiet High-Resolution Computer Models of a Plasma. *J. Comput. Phys.* **1974**, *14*, 148−158.

https://doi.org/10.1021/acs.jpcc.3c04661
J. Phys. Chem. C 2023, 127, 16740−16750